LBL-36629
UC-405

Lawrence Berkeley Laboratory
UNIVERSITY OF CALIFORNIA

Physics Division
Mathematics Department

Presented at the AIAA Aerospace Sciences Meeting,
Reno, NV, January 9–12, 1995, and to be published
in the Proceedings

On Cylindrical Container Sections for a Capillary Free-Surface Experiment

A. Chen, P. Concus, and R. Finn

January 1995

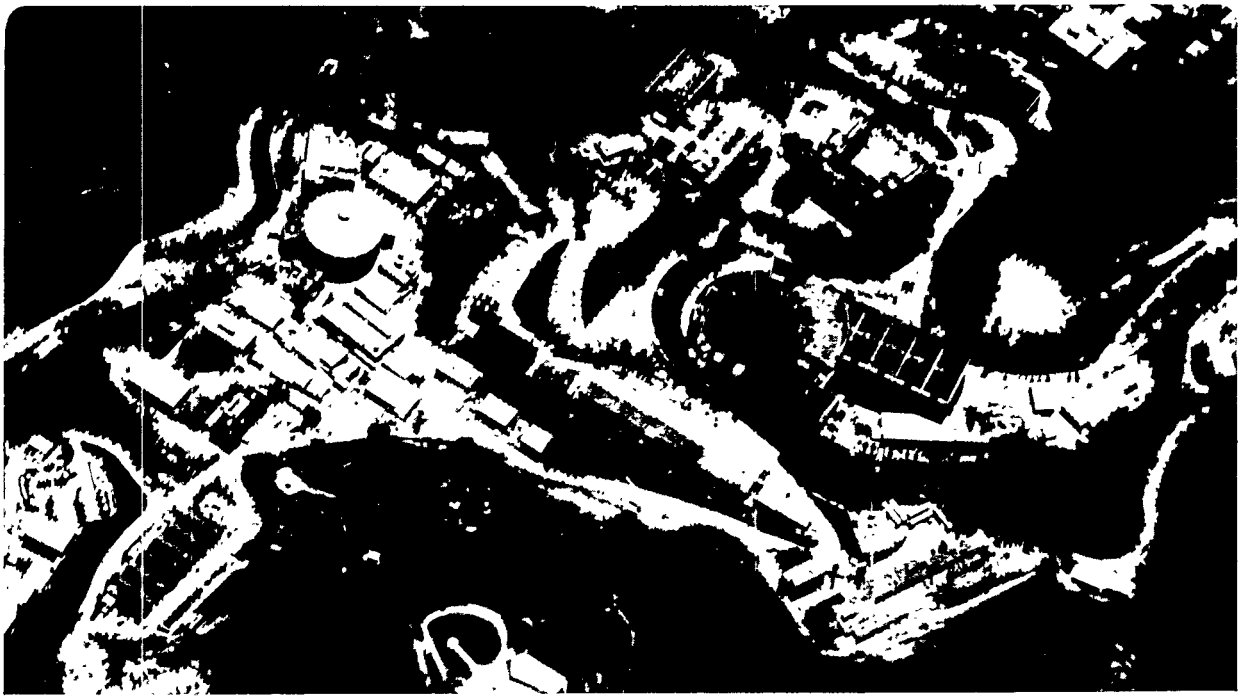

Prepared for the U.S. Department of Energy under Contract Number DE-AC03-76SF00098

LBL-36629
AIAA 95-0271

ON CYLINDRICAL CONTAINER SECTIONS FOR A CAPILLARY FREE-SURFACE EXPERIMENT*

Allen Chen
Department of Mathematics
University of California
Berkeley, CA 94720

Paul Concus
Lawrence Berkeley Laboratory
and
Department of Mathematics
University of California
Berkeley, CA 94720

Robert Finn
Department of Mathematics
Stanford University
Stanford, California 94305

January 1995

*This work was supported in part by the National Aeronautics and Space Administration under Grants NAG3-1143 and NCC3-329, by the National Science Foundation under Grant DMS91-06968, and by the Mathematical Sciences Subprogram of the Office of Energy Research, U. S. Department of Energy, under Contract Number DE-AC03-76SF00098.

ON CYLINDRICAL CONTAINER SECTIONS FOR A CAPILLARY FREE-SURFACE EXPERIMENT

Allen Chen*
University of California, Berkeley, CA 94720

Paul Concus†
Lawrence Berkeley Laboratory and
University of California, Berkeley, CA 94720

Robert Finn‡
Stanford University, Stanford, CA 94305

Abstract

Small changes in container shape or in contact angle can give rise to large shifts of liquid in a microgravity environment. These shifts can be used as a basis for accurate determination of contact angle. We describe container shapes, designed for a forthcoming USML-2 experiment, in the form of a circular cylinder with two diametrically opposed "canonical proboscis" protrusions. Computational studies indicate that these containers can be designed to have the desirable properties that sufficient liquid will participate in the shift to permit easy observation, but that the change will be abrupt enough to allow precise contact angle determination.

Introduction

When planning space-based operations, it is important to be able to predict the locations and configurations that fluids will assume in containers under low-gravity conditions. For example, one could be in serious difficulty if one did not know in advance where the fuel is to be found in a spacecraft's partially filled fuel tank. Currently available mathematical theory applies completely, however, to only a few particular configurations, such as the partially filled right circular cylindrical container with the fluid simply covering the base. For such a configuration, behavior in space is not dramatically different from what is familiar from common experience in a terrestrial environment. For more general containers, however, fluids in reduced gravity can behave in striking, unexpected ways.

The classical theory, according to the Young-Laplace-Gauss formulation, characterizes fluid locations as equilibrium configurations for the surface-plus-gravitational mechanical energy. Using this point of view in a mathematical study, we have shown that for a cylindrical container of general cross-section in zero gravity the surface change arising from small changes in geometry or contact angle can be discontinuous or "nearly discontinuous", leading to large shifts of the liquid mass. This behavior can be exploited as a means for accurate determination of contact angle.

The principal mathematical result underlying the behavior is that for particular cylindrical sections a discontinuous kind of change can be realized as the contact angle γ crosses a critical value γ_0 intrinsic to the container. When γ is larger than γ_0 there exists an equilibrium configuration of liquid that covers the base of the cylindrical container simply, while for contact angles smaller than γ_0 no such equilibrium configuration is possible. In the latter case fluid moves to the walls and can rise arbitrarily high along a part of the wall, uncovering a portion of the base if the container is tall enough. By simple observation of bulk behavior of the fluid, one can thereby determine whether the contact angle is larger than or smaller than the critical value for the container. A practical challenge in this connection is to design cross-sections for which a large enough portion of the fluid will rise up the walls for easy observation as the critical value of contact angle is crossed, without the containers being unrealistically tall, and so that the change will be abrupt enough to make the contact angle determination precise.

By using two or more containers corresponding to appropriately chosen values of γ_0, differing, say, by the accuracy desired for a contact angle evaluation, one can determine the value of the contact angle to lie within a particular interval. In some cases, geometries can be "combined" into a single container for determining such an interval. For our

* Graduate Student, Department of Mathematics

† Senior Scientist, Lawrence Berkeley Laboratory and Adjunct Professor, Department of Mathematics

‡ Professor, Department of Mathematics

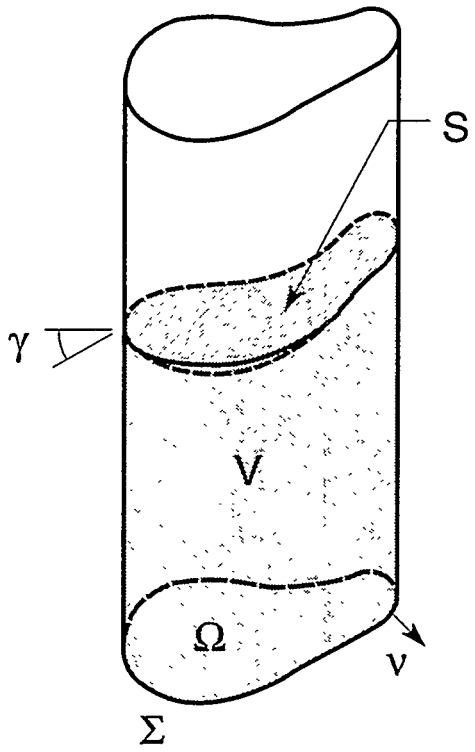

Figure 1. Partly filled cylindrical container with base Ω.

planned Interface Configuration Experiment (ICE) on the second Unites States Microgravity Laboratory flight (USML-2), in collaboration with Mark Weislogel of NASA Lewis Research Center, we conjoin these two approaches.

Governing equations

Consider a cylindrical container of general cross-section partly filled with liquid, as indicated in Fig. 1. According to the classical theory, an equilibrium interface in the absence of gravity between the liquid and gas (or between two immiscible liquids) is determined by the equations

$$\operatorname{div} Tu = \frac{1}{R_\gamma} \quad \text{in } \Omega, \tag{1}$$

$$\nu \cdot Tu = \cos\gamma \quad \text{on } \Sigma, \tag{2}$$

where

$$Tu \equiv \frac{\nabla u}{\sqrt{1+|\nabla u|^2}};$$

see, e. g., Chap. 1 of Ref. 1. In these equations Ω is the cross section (base) of the cylindrical container, Σ is the boundary of Ω, ν is the exterior unit normal on Σ, and

$$R_\gamma = \frac{|\Omega|}{|\Sigma|\cos\gamma}, \tag{3}$$

where $|\Omega|$ and $|\Sigma|$ denote respectively the area and length of Ω and Σ; $u(x,y)$ denotes the height (single-valued) of the interface S above a reference plane parallel to the base, and γ is the contact angle between the interface and the container wall, determined by the material properties. The volume V of liquid in contact with the base is assumed to be sufficient to cover the base entirely, and, for the mathematical results, the cylinder is assumed implicitly to be arbitrarily tall so that questions of behavior at a top do not arise. We restrict discussion here to the case of a wetting liquid $0 \le \gamma < \pi/2$ (the complementary non-wetting case can be easily transformed into this one). For $\gamma = \pi/2$, the solution surface is a horizontal plane for any cross-section.

Wedge container

For a cylindrical container whose section Ω contains a protruding corner with opening angle 2α, as in Fig. 2, the critical value of contact angle is $\gamma_0 = \frac{\pi}{2} - \alpha$. For $\frac{\pi}{2} > \gamma \ge \gamma_0$ (and for fluid volume sufficient to cover the base) the height u can be given in closed form as the portion of the lower hemisphere with center at O meeting the walls with the prescribed contact angle γ. Thus the height is bounded uniformly in γ throughout this range. For $0 \le \gamma < \gamma_0$, however, the fluid will necessarily move to the corner and rise arbitrarily high at the vertex, uncovering the base regardless of fluid volume. The behavior for the wedge domain is thus discontinuous at $\gamma = \gamma_0$. Background details and historical discussion of this behavior are given in Refs. 1, 2, 3, and references cited there. Procedures for determining contact angle based on the phenomenon can give very good accuracy for larger values of γ (closer to $\pi/2$) but may be subject to experimental inaccuracy when γ is closer to zero, as the "singular"

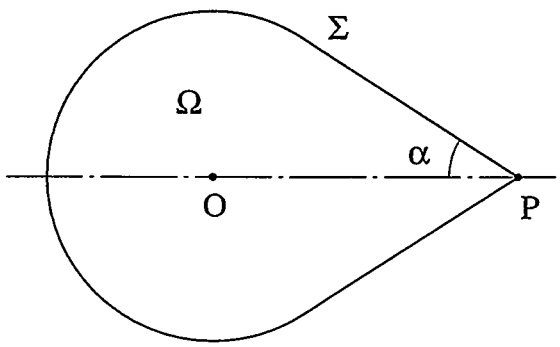

Figure 2. Wedge container section.

part of the section over which the fluid accumulates when the critical angle γ_0 is crossed then becomes very small and may be difficult to observe.

Canonical proboscis container

As a way to overcome the experimental difficulty, "canonical proboscis" sections were introduced in Ref. 4. These domains consist of a circular arc attached symmetrically to a (symmetric) pair of curves described by

$$x+C = \sqrt{{R_0}^2 - y^2} + R_0 \sin\gamma_0 \cdot \ln \frac{\sqrt{{R_0}^2 - y^2}\cos\gamma_0 - y\sin\gamma_0}{R_0 + y\cos\gamma_0 + \sqrt{{R_0}^2 - y^2}\,\sin\gamma_0}, \quad (4)$$

and meeting at a point P on the x-axis, see Fig. 3. Here R_0, as well as the particular points of attachment, may be chosen arbitrarily. The (continuum of) circular arcs Γ_0, of which three are depicted by the dashed curves in Fig. 3, are all horizontal translates of one such arc, of radius R_0 and with center on the x-axis, and the curves (4) have the property that they meet all the arcs Γ_0 in the constant angle γ_0. If the radius ρ of the circular boundary arc can be chosen in such a way that R_0 is the value of R_γ from (3) for the value $\gamma = \gamma_0$, then the arcs Γ_0 become extremals for a "subsidiary" variational problem[5] (see also Ref. 1, Chap. 6 and Ref. 2) determined by the functional

$$\Phi \equiv |\Gamma| - |\Sigma^*|\cos\gamma + |\Omega^*|/R_\gamma \quad (5)$$

defined over piecewise smooth arcs Γ, where Σ^* and Ω^* are the portions cut off from Σ and Ω by the arcs. In the case of the section of Fig. 3, Σ^* and Ω^* lie to the right of the indicated arcs. It can be shown[5,1] that every extremal for Φ is a subarc of a semicircle of radius R_0, with center on the side of Γ exterior to Ω^*, and that it meets Σ in angles $\geq \gamma_0$ on the side of Γ within Ω^*, and $\geq \pi - \gamma_0$ on the other side of Γ (and thus in angle γ_0 within Ω^* whenever the intersection point is a smooth point of Σ). It is remarkable that whenever (3) holds, $\Phi = 0$ for every Ω^* that is cut off in the proboscis by one of the arcs Γ_0; see Ref. 4 and the references cited there.

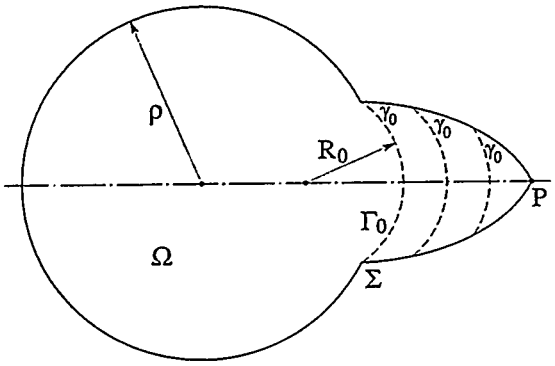

Figure 3. Proboscis container section showing three members of the continuum of extremal arcs.

In Ref. 4, a value for ρ was obtained empirically from (3) in a range of configurations, and it was conjectured that the angle γ_0 on which the construction is based would be critical for the geometry. That is, a solution of (1), (2), (3) should exist in Ω if and only if $\gamma > \gamma_0$. Additionally, the fluid height should rise unboundedly as γ decreases to γ_0, precisely in the region swept out by the arcs Γ_0 (the entire proboscis region to the right of the leftmost arc Γ_0 shown in Fig. 3). For these conjectures, which form the basis of our proposed procedure and for which the mathematical underpinnings were proved only partially in Ref. 4, complete mathematical proofs have been carried out.[6] Specifically, it has been established that a unique value of ρ can be obtained for any specified proboscis length and that the conjectured behavior of the fluid rise is the only one possible.

In Ref. 7 numerical solutions of (1), (2), (3) are depicted for some canonical proboscis containers. Although the fluid rise in the corner is not discontinuous as occurs for a planar wedge, it can be "nearly discontinuous" in that the rise height in the proboscis is relatively modest until γ decreases to values close to γ_0, and then becomes very rapid at $\gamma = \gamma_0$. Furthermore, since the proboscis can be made relatively as large a portion of the section as desired, the shift can be easily observed for a broad range of γ_0. Through proper choice of the domain parameters for the cases considered, an effective balance can be obtained between conflicting requirements of a sharp near discontinuity (for accurate measurement) and a sizable volume of fluid rise (for ease of observation).

Double proboscis container

For the USML-2 experiment, double proboscis containers will be used. These containers are similar to the single proboscis one of Fig. 3, except that there is a second proboscis diametrically opposite to the first, in effect combining two containers into one. The values of γ_0 in (4) generally differ for the left and right proboscides, whose values of γ_0 we denote by γ_L and γ_R, respectively. Similarly, we denote the values of R_0 for the left and right

proboscides by R_L and R_R. In order for (3) to be satisfied for both proboscides, there holds

$$R_R \cos\gamma_R = R_L \cos\gamma_L.$$

Specifying the desired points of attachment and choosing ρ, the radius of the circular portion of the section, so that (3) is satisfied then yields the container section. (Such a ρ can be chosen for the cases considered here, but a proof that such a choice is possible for any proboscis lengths has not yet been carried out for the double proboscis case.) The critical value for the container is the larger of γ_L and γ_R. For the containers considered here, we shall take $\gamma_R > \gamma_L$, so that the critical contact angle γ_0 for the container is equal to γ_R.

The upper half of the sections for the experiment, superimposed on one another, are shown in Fig. 4. The sections have been scaled so that the circular portions all have radius unity. The meeting points of the vertices with the x-axis are, respectively, a distance 1.5 and 1.6 from the circle center. For the sections depicted in Fig. 4 the values of γ_L and γ_R are respectively 20° and 26° for the uppermost section, 30° and 34° for the middle section, and 38° and 44° for the lowest section.

For these containers the explicit behavior has not yet been determined mathematically in complete detail, as it has for the single proboscis containers. However, numerical computations discussed below and the known behavior of the single proboscis solution surfaces suggest that the behavior will be as follows: For contact angles $\gamma \geq \gamma_0$, as γ decreases to γ_0 the fluid will rise higher in the right than in the left proboscis, with the rise becoming unbounded in the right proboscis at γ_0. For contact angles between γ_L and γ_R the fluid will rise arbitrarily high in the right proboscis, but the height in the left will still be bounded. For smaller contact angles the fluid will rise up both proboscides arbitrarily high. By observing the liquid shift, one can then bracket the contact angle relative to the values of γ_L and γ_R. For a practical situation in which the container is of finite height with a lid on the top, the fluid will rise to the lid along one or both of the proboscides in the manner described above (providing the fluid volume is adequate).

The selected values of γ_L and γ_R for the three containers are based on the value of approximately 32° measured in a terrestrial environment for the contact angle between the experiment fluid and the acrylic plastic material of the container. The spread of values of contact angle covered by the three containers is intended to allow observation of possible effects of contact angle hysteresis, which is not included in the classical theory.

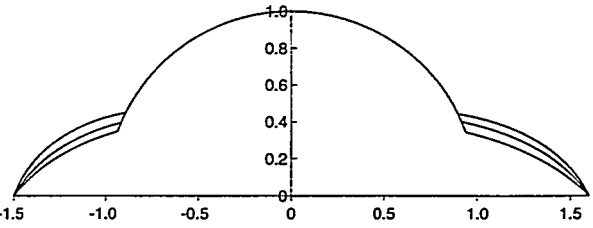

Figure 4. Three superimposed double proboscis container sections. From uppermost to lowest, the pair of values of γ_0 for the left and right proboscides of each section are 20°/26°, 30°/34°, and 38°/44°.

Numerical results

Eqs. (1), (2), (3) were solved numerically for the three double proboscis container sections depicted in Fig. 4, for a range of contact angles γ, to obtain details of the anticipated fluid behavior. The adaptive-grid finite-element software package PLTMG[8] was used for computing the numerical solution. As input to the package, which accepts linear or circular-arc boundary segments, the proboscis portions of the boundary were approximated by piecewise-linear segments. The circular-arc portions could be represented as such.

To speed the computation, only the upper half domains shown in Fig. 4 were input to PLTMG, with reflective symmetry boundary condition $\nu \cdot \nabla u = 0$ in place of (2) along the symmetry line. Solutions were normalized by taking $u = 0$ at the center of the unit circle portion of the domain boundary.

The numerically calculated solution surface $u(x, y)$ for (the upper half of) the 30°/34° domain is shown in Fig. 5 for four values of contact angle, 60°, 50°, 40°, and 35°. (The critical value for the domain is $\gamma_0 = 34°$.) The three-dimensional views of the surface are color-shaded by PLTMG to indicate contour levels, grayscale versions of which are shown in the figure. The viewpoint for each surface is the same. Generally, the computations indicate that as γ decreases toward the critical contact angle, fluid moves toward and up the two proboscis walls, with the local maximum heights, as calculated by the program, at the proboscis tips. The heights at the right are higher than the corresponding ones at the left. The surfaces for the 20°/26°

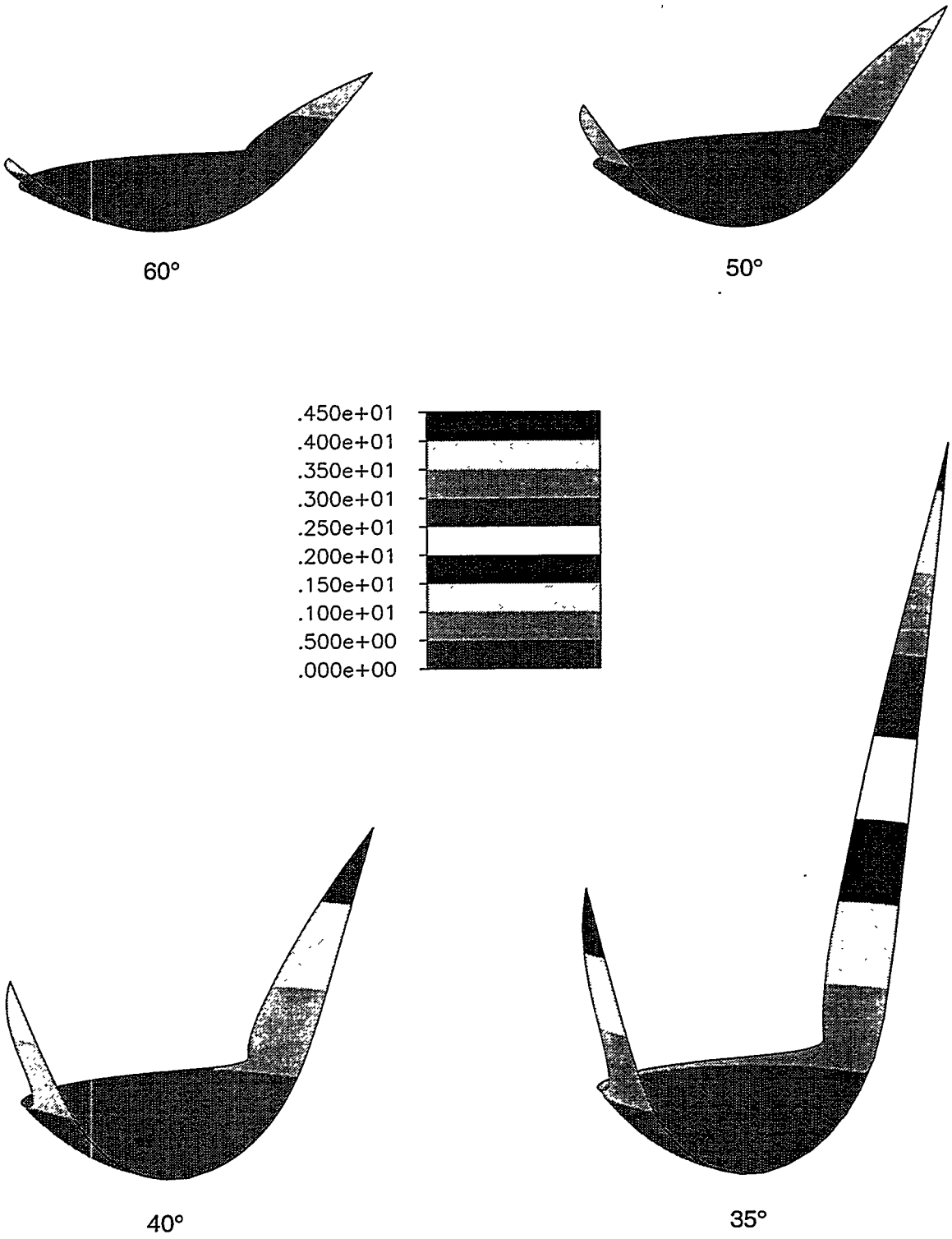

Figure 5. Equilibrium interface for the 30°/34° (upper-half) double proboscis section for contact angles 60°, 50°, 40°, and 35°. $\gamma_0 = 34°$.

and 36°/44° proboscis domains behave similarly.

The apparent jump discontinuity in the solution height at the reentrant corners occurs in the computed solutions for contact angles smaller than a certain value, depending on the domain. (For the solutions depicted in Fig. 5 compare the surface for 60° with the others.) Such discontinuous behavior for solutions of (1), (2), (3) at reentrant corners has been characterized mathematically for certain domains in a recent study.[9] The effect of this behavior on the numerical computations in PLTMG was evidenced in the adaptive mesh refinement. Higher levels of refinement concentrated nodes in the neighborhood of the reentrant corners. Thus with the approximately 6000 nodes to which we limited the computation, relatively fewer nodes were distributed elsewhere in the domain than was the case when the discontinuities were not present. The estimate of the L^2 norm of the error given by PLTMG was, nonetheless, the order of 10^{-2} or less in all cases. Based on comparison of numerical solutions for problems with the number of interior mesh nodes varying from 2000 to 6000 and the number of piecewise-linear segments approximating each proboscis varying from 20 to 30, we estimate that the errors in the values of the maximum heights and volumes in Fig. 5 to be less than about 3%.

The heights at the proboscis tips are shown as a function of γ for the three domains by the solid curves in the left of Fig. 6. The volume of the liquid rising above the minimum point of the surface is depicted on the right. The calculated data, which are denoted by "+" for the right proboscis and "○" for the left, are connected by interpolating linear segments. For each container, the leftmost calculated point is for a value of γ that is 1/2 degree greater than the critical value. At the critical values $\gamma = \gamma_0$ (26°, 34°, and 44° respectively), denoted by the arrows, the right tip heights and the volumes would become infinite. Four of the calculated points for the 30°/34° domain are the ones corresponding to the surfaces shown in Fig. 5.

For comparison, the dashed curves in the left of Fig. 6 show the rise height at the boundary for a circular domain with no protrusions, for which the solution is the lower spherical cap

$$u(x,y) = \left(1 - \sqrt{1 - (x^2+y^2)\cos^2\gamma}\right)\sec\gamma,$$

which has its minimum at the origin and maximum $(\sec\gamma - \tan\gamma)$ at the boundary.

One sees that the rise heights in the containers are modest until γ gets close to the critical value. Fig. 6 indicates that by using a container of height 5, say, one could distinguish between the critical value γ_0 for the container (fluid in right proboscis rises to the lid) and a contact angle value one degree greater (fluid rise height < 5). By using taller containers one might determine critical values with even greater precision.

ICE experiment

In addition to the three double proboscis containers depicted in Fig. 4, the USML-2 ICE experiment has also a wedge container. This container is constructed to allow the interior wedge angle 2α (see Fig. 2) to be varied, so as to permit observation of the wedge phenomenon for both the advancing and receding cases. It is anticipated that the experiment will indicate to what extent mathematically predicted behavior can be observed in practice, and also that it will shed light on effects not included in the classical theory, such as those associated with contact-line resistance forces.

Acknowledgments

We wish to thank Mark Weislogel for numerous discussions and Randolph Bank for his personal guidance in use of the PLTMG software package. This work was supported in part by the National Aeronautics and Space Administration under Grants NAG3-1143 and NCC3-329, by the National Science Foundation under Grant DMS91-06968, and by the Mathematical Sciences Subprogram of the Office of Energy Research, U. S. Department of Energy, under Contract Number DE-AC03-76SF00098.

References

[1]R. Finn, *Equilibrium Capillary Surfaces*, Springer-Verlag, New York, 1986. Russian translation (with Appendix by H.C. Wente) Mir Publishers, 1988.

[2]P. Concus and R. Finn, *Dichotomous behavior of capillary surfaces in zero gravity*, Microgravity Sci. Technol. 3 (1990), pp. 87–92; Errata, 3 (1991), p. 230.

[3]P. Concus and R. Finn, *Capillary surfaces in microgravity*, in *Low-Gravity Fluid Dynamics and Transport Phenomena*, J. N. Koster and R. L. Sani, eds., Progress in Astronautics and Aeronautics, Vol.

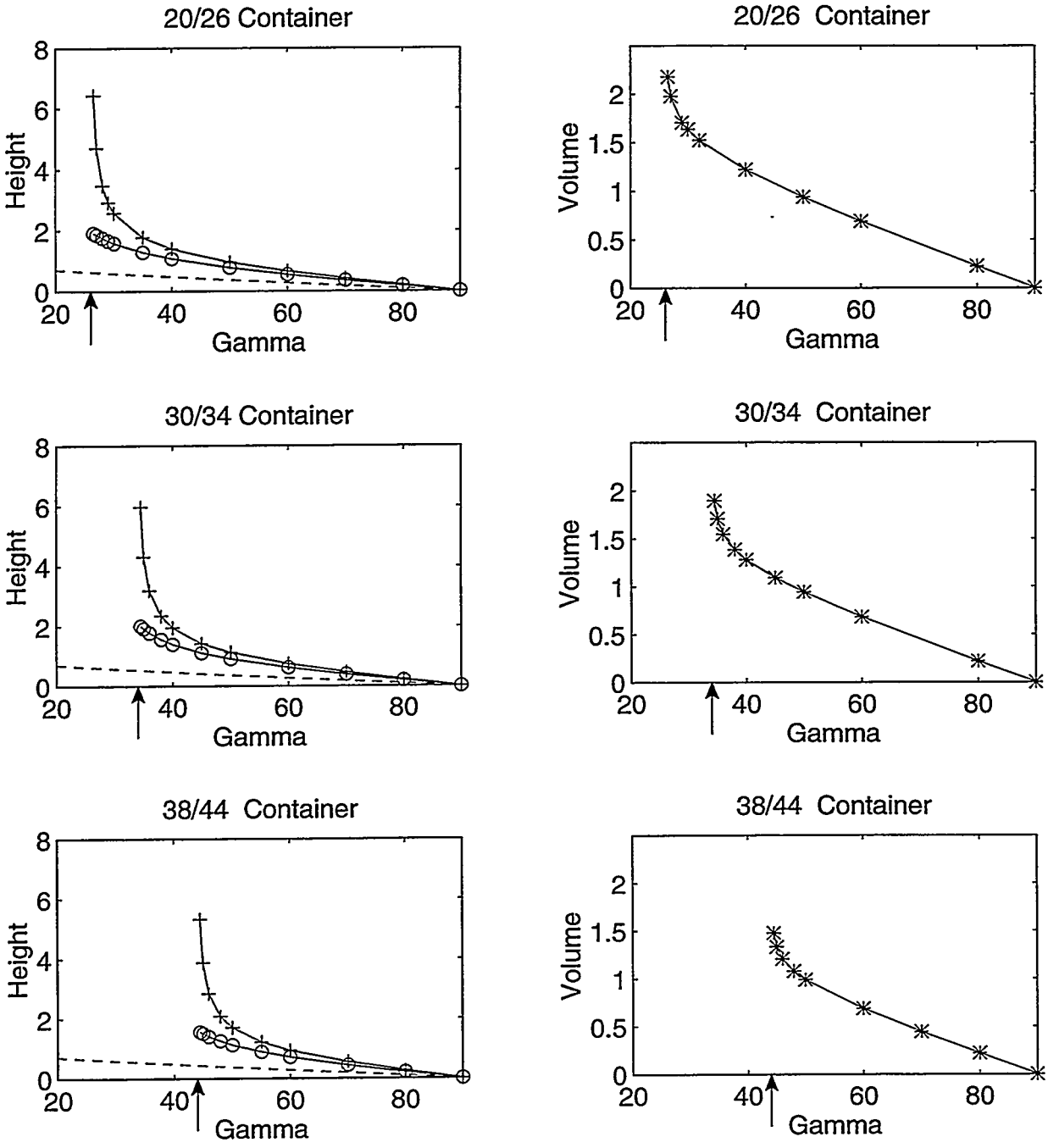

Figure 6. Rise heights at right (+) and left (○) proboscis tips and total volume of rise vs. contact angle for the three container sections. $\gamma_0 = 26°$, 34°, and 44°, respectively, as denoted by the arrows.

130, AIAA, Washington, DC, 1990, pp. 183–206.

[4]B. Fischer and R. Finn, *Non-existence theorems and measurement of capillary contact angle*, Zeit. Anal. Anwend. 12 (1993), pp. 405–423.

[5]R. Finn, *A subsidiary variational problem and existence criteria for capillary surfaces*, J. reine angew. Math. 353 (1984), pp. 196–214.

[6]R. Finn and T. Leise, *On the canonical proboscis*, Zeit. Anal. Anwend. 13 (1994), pp. 443-462.

[7]P. Concus, R. Finn, and F. Zabihi, *On canonical cylinder sections for accurate determination of contact angle in microgravity*, in *"Fluid Mechanics Phenomena in Microgravity"*, AMD Vol. 154, Amer. Soc. Mech. Engineers, D. A. Siginer and M. M. Weislogel, eds., New York, 1992, pp. 125–131.

[8]R. E. Bank, PLTMG: A Software Package for Solving Elliptic Partial Differential Equations, SIAM, Philadelphia, 1994; software available via Netlib (WWW: `http://www.netlib.org`, E-mail: `netlib@research.att.com`).

[9]K. Lancaster and D. Siegel, *Radial limits of capillary surfaces*, to appear.